Structure, Vol. 12, 2081–2093, November, 2004, ©2004 Elsevier Ltd. All rights reserved. DOI 10.1016/j.str.2004.08.014

The X-Ray Structure of RANTES: Heparin-Derived Disaccharides Allows the Rational Design of Chemokine Inhibitors

Jeffrey P. Shaw,[1,*] Zoë Johnson,[1,4] Frédéric Borlat,[1] Catherine Zwahlen,[2] Andreas Kungl,[3] Karen Roulin,[1] Axel Harrenga,[1,5] Timothy N.C. Wells,[1] and Amanda E.I. Proudfoot[1,*]

[1]Serono Pharmaceutical Research Institute
14 Chemin des Aulx
1228 Plan-les-Ouates
Geneva
Switzerland

[2]GeneProt
2 Rue du Pré-de-la-Fontaine
1217 Meyrin
Switzerland

[3]Department of Protein Chemistry and Biophysics
Institute of Pharmaceutical Chemistry
and Pharmaceutical Technology
University of Graz
A-8010 Graz
Austria

Summary

The biological activity of chemokines requires interactions with cell surface proteoglycans. We have determined the structure of the chemokine RANTES (regulated on activation normal T cell expressed) in the presence of heparin-derived disaccharide analogs by X-ray crystallography. These structures confirm the essential role of the BBXB motif in the interaction between the chemokine and the disaccharide. Unexpected interactions were observed in the 30s loop and at the amino terminus. Mutant RANTES molecules were designed to abrogate these interactions and their biological activity examined in vivo. The K45E mutant within the BBXB motif lost the capacity to bind heparin and the ability to elicit cellular recruitment. The Y3A mutant maintained its capacity to bind heparin but was unable to elicit cellular recruitment. Finally, a tetrasaccharide is the smallest oligosaccharide which effectively abolishes the ability of RANTES to recruit cells in vivo. These crystallographic structures provide a description of the molecular interaction of a chemokine with glycosaminoglycans.

Introduction

The chemokine family is composed of approximately 40 members whose role is to direct cellular migration through interaction with receptors of the seven transmembrane G protein coupled receptor family. RANTES (regulated on activation normal T cell expressed) (CC chemokine ligand 5 [CCL5]), a member of the CC or β subclass, is a highly basic, 68 amino acid protein, which induces migration of T cells, monocytes, basophils, eosinophils, natural killer cells, and dendritic cells (Baggiolini et al., 1997) by binding to several receptors, namely CCR1, CCR3, and CCR5 (Rossi and Zlotnik, 2000). Overexpression of RANTES has been associated with a variety of inflammatory disorders (Folkard et al., 1997; Robinson et al., 1995).

The immobilization of chemokines by interaction with proteoglycans on cell surfaces and the extracellular matrix (Sweeney et al., 2002) is essential for their ability to induce directional migration (Proudfoot et al., 2003). In vitro, several chemokines have been shown to bind to glycosaminoglycans (GAGs), such as heparin, heparin sulfate, chondroitin sulfate, and dermatan sulfate (Hoogewerf et al., 1997). In these in vitro studies, RANTES displayed the widest range of affinities across the different GAGs and has a particularly high affinity for heparin (Kuschert et al., 1999). Mutagenesis studies on RANTES have shown that the interaction of RANTES and heparin is mediated principally through the highly basic BBXB motif ^{44}RKNR^{47}, located on the 40s loop exposed on the surface of the protein (Proudfoot et al., 2001). The RANTES-^{44}AANA^{47} mutant still binds its CCR5 receptor with wild-type affinity, but its affinity for its CCR1 is decreased 200-fold (Proudfoot et al., 2001; Martin et al., 2001), demonstrating that the heparin binding sites can, in some cases, overlap with the receptor binding site.

Certain chemokines, such as IL-8 (Rajarathnam et al., 1994), MCP-1 (Paavola et al., 1998), MIP-1β (Laurence et al., 2000), and RANTES (Proudfoot et al., 2003), have been shown to achieve full receptor activation as monomers, although they also form stable dimers. RANTES displays a marked propensity to oligomerize into higher order complexes at high concentrations, high pH, or in the presence of heparin (Czaplewski et al., 1999; Stura et al., 2002). Mutants of RANTES, MCP-1, and MIP-1β with either reduced affinity to heparin, or an abrogated propensity to form dimers and higher-order oligomers, lose their in vivo capacity to recruit leukocytes despite being fully capable of binding their receptor in vitro (Proudfoot et al., 2003).

Recently, the glycosaminoglycan-cytokine interaction has also become recognized as a therapeutic target in such applications as graft rejection (Fernandez-Botran et al., 2002), and considerable efforts are now underway to characterize the heparin binding domains of chemokines (Koopmann et al., 1999; Chakravarty et al., 1998; Stringer and Gallagher, 1997; Stringer et al., 2002; Spillmann et al., 1998). Moreover, mutation of the GAG binding site of RANTES has revealed a novel anti-inflammatory strategy, since mutation of the basic residues in the BBXB heparin binding motif on the 40s loop (RANTES-^{44}AANA^{47}) has been shown to prevent cellular recruitment by wild-type RANTES (Baltus et al., 2003), and furthermore, significantly reduces symptoms in a murine model of inflammation, experimental autoimmune encephalomyelitis (Johnson et al., 2004).

In order to more fully understand which residues in

*Correspondence: jeffrey.shaw@serono.com
[4]Current address: Celltech, 216 Bath Road, Slough, Berkshire SL1 4EN, United Kingdom.
[5]Current address: Astex Technology, 436 Cambridge Science Park, Milton Road, Cambridge CB4 0QA, United Kingdom.

RANTES are directly implicated in binding to glycosaminoglycans and to understand the structure of the higher-order oligomerization states of RANTES in their presence, the cocrystallization of RANTES with glycosaminoglycan-derived fragments was undertaken. The crystal structure of RANTES complexed to heparin-derived disaccharides I-S and III-S were obtained. These structures confirmed the important role of the BBXB motif in the 40s loop in binding to glycosaminoglycans, but identified several other unexpected interactions with the 30s loop, and the N terminus. Residues within these regions which interacted with the disaccharides in the crystal structure were mutated to residues which could not maintain this interaction, and their in vivo activity determined.

Results

Structure of Wild-Type RANTES and Heparin-Derived Disaccharides

The structure of wild-type RANTES and variants had previously been determined by both NMR (Skelton et al., 1995; Chung et al., 1995) and X-ray crystallography (Hoover et al., 2000; Wilken et al., 1999). In all cases the protein is a homodimer of monomers (hereafter called monomer A and monomer B) consisting of an NH_2-terminal loop, three antiparallel β strands arranged in a Greek key motif, connected by loops, and a COOH-terminal α helix, which is the generic monomeric structure of all chemokines. The two crystallographic structures also contained several sulfate ions either near the BBXB loop or near the dimer interface. Our assumption was that the positions of these sulfate ions would reveal the binding site of the sulfate groups of heparan sulfate. Heparin and heparan sulfate are long unbranched oligosaccharides composed of variously sulfated disaccharide building blocks (Figure 1). These disaccharide building blocks are composed of a hexuronic acid moiety and a D-glucosamine subunit linked by 1 → 4 linkages. The uronic acid may either be β-D-glucuronic acid or α-L-iduronic acid and can either be underivatised or 2-O-sulfated. The α-D-glucosamine residue may be either N-sulfated or N-acetylated. The N-sulfated glucosamines may also be O-sulfated at C3, C6, or both, or may not be O-sulfated at all. The N-acetylated glucosamines may be O-sulfated at C6 or may be O-unsulfated. Thus each disaccharide monomer has one of six possible structures in the glucosamine position, and four possible structures in the glucuronic acid position.

Since heparin is such a large polydisperse molecule, it was concluded that initial studies should be undertaken with the much smaller, chemically well-characterized building blocks of the heparin polymer, such as sulfated D-glucosamines, hexuronic acids, and heparin-derived oligosaccharides. Since RANTES was found to precipitate in the presence of heparin-derived fragments larger than a disaccharide and since these heparin-derived disaccharides are readily available, are chemically pure, and are chemically very similar to the smallest building blocks of heparin molecules, they were chosen for this study. It should be noted, however, that the commercially available heparin-derived disaccharides are produced by the action of heparin lyases that cleave heparin between glucosamine residues and their downstream uronic acids. These lyases produce disaccharides with a nonnatural unsaturated $\Delta^{4,5}$-uronic acid at its nonreducing terminal. This unsubstituted uronic acid is thus structurally different from the uronic acid present in the heparin polysaccharide and care must therefore be taken in the interpretation of the significance of the interactions of this $\Delta^{4,5}$-uronic acid moiety with RANTES.

Cocrystallization of wild-type RANTES in presence of these heparin-derived disaccharides was attempted. Crystals grew in all cases except in the presence of heparin disaccharide I-A and IV-S (Table 1). The crystals of RANTES grown in the presence of the heparin-derived disaccharides were all isomorphous to the wild-type protein crystals. Unexpectedly, only disaccharides I-S and III-S (which only differ by the presence of an O-sulfate group at position C6 of the glucosamine moiety of disaccharide I-S) were visible in the crystal structure, whereas heparin-derived disaccharides II-A and II-S (which lack the sulfate group on the C2′ of the glucuronic moiety) were not present in the crystals grown in their presence.

The overall structure of the RANTES molecule is unaffected by the presence of the heparin-derived disaccharide molecules, with the exception of the N terminus of the B monomer of the RANTES dimer (Figure 2) in the structure containing heparin-derived disaccharide I-S. The rms deviation of the position of the main chain atoms between residues 6 and 72 (excluding therefore the very mobile N-terminal region) of Met-RANTES and RANTES containing heparin disaccharides I-S and III-S is 0.6 Å and 0.52 Å, respectively. Residues 2–68 are visible for monomer A of both heparin-derived disaccharide I-S and III-S containing crystals, whereas only residues 4–68 are visible for both B monomers. There is a single heparin disaccharide I-S or III-S molecule in the asymmetric unit, which contains a dimer of RANTES. The disaccharides are nestled between three symmetry-related dimers of RANTES and form either salt bridges or hydrogen bond interactions with all three (Figure 3). The disaccharide interacts with residues at the N terminus of monomer A of the first RANTES dimer and with residues of a solvent-exposed loop composed of residues Ser31A to Lys33A (hereafter called the 30s loop). This disaccharide also interacts with residues His23B, Arg44B, and K45B (part of the 40s loop) of the B monomer of a second RANTES dimer, which is symmetry-related to the first. A third, symmetry-related RANTES dimer, interacts with this disaccharide through residues Thr8B and Gly32B of the B monomer. The N termini and the 30s loops of both monomers are important for RANTES-disaccharide interaction, as well as the two residues of the BBXB motif previously identified as playing an important role in heparin binding (Proudfoot et al., 2001). The N terminus of the A monomer of RANTES forms only one important hydrogen bond to the disaccharide, through the OH of the side chain of Tyr3A. Probably as a consequence of this tight hydrogen bond, the entire N-terminal main chain moves toward the heparin disaccharide, with the most movement occurring at the extreme end of the RANTES N terminus. The Tyr3A side chain also undergoes an important change in posi-

A

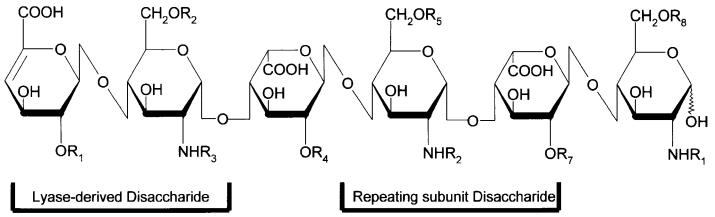

Figure 1. Structure of Heparin

(A) Heparin polysaccharide structure.
(B) Heparin-derived disaccharide structure.
(C) Nomenclature of heparin disaccharides.

B

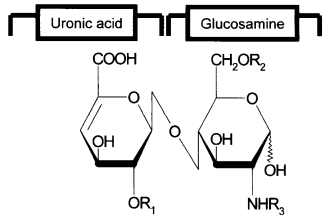

C

Heparin Disaccharide	R1	R2	R3
I-S	$-SO_3^-$	$-SO_3^-$	$-SO_3^-$
II-S	-	$-SO_3^-$	$-SO_3^-$
III-S	$-SO_3^-$	-	$-SO_3^-$
IV-S	-	-	$-SO_3^-$
I-A	$-SO_3^-$	$-SO_3^-$	$-COCH_3$
II-A	-	$-SO_3^-$	$-COCH_3$
III-A	$-SO_3^-$	-	$-COCH_3$
IV-A	-	-	$-COCH_3$

tion and swings around, with the OH group forming a hydrogen bond with the 2′-sulfate group of the hexuronic acid moiety of the disaccharide. This interaction is further stabilized by a hydrogen bond between the OH group of Tyr3A and the Oγ of Ser31A, an interaction not observed in the AOP and Met-RANTES structures (Wilken et al., 1999; Hoover et al., 2000). The importance of the interaction of the Tyr3 side chain with the heparin disaccharide prompted the preparation and characterization of the RANTES-Y3A mutant described below. The side chain of Ser4A apparently does not swing around to interact with the disaccharide 2′-SO_4 group, despite being well within range to form a hydrogen bond with the 2′-SO_4 group of the hexuronic moiety of the disaccharide. The side chain of Thr8A also swings around, compared to AOP-RANTES or Met-RANTES structures, and forms two hydrogen bonds with two oxygen atoms of the 2′-SO_4 group of the hexuronic acid.

The N terminus of the B-chain of the RANTES dimer undergoes a much more pronounced movement than the N terminus of the A-chain, despite the lack of any direct interaction with the disaccharides. This N terminus rotates around the Asp6B Cα-CO bond, with the side chain pointing in the direction of the main chain in the AOP and Met-RANTES structures. Residues 1–3 are not visible in the electron density, and this movement was only visible for residues 4–6. This movement was not observed in the structure containing heparin disaccharide III-S, and results in the lengthening of the N-terminal β strand of the B chain by two amino acids (residues Ser4B and Ser5B). The new position of the Asp6B side chain also creates two new hydrogen bonds with the main chain N of Cys50A, which may play a role in stabilizing the RANTES dimer upon binding of heparin. Since none of residues 4B–6B bind directly to the heparin disaccharide, and there are no steric reasons for the movement of the N terminus, it is not entirely clear why the movement should take place, unless it is simply due to modified packing in the crystal lattice to allow the presence of the disaccharide.

Several residues in the 30s loop form interactions either with the disaccharides or within the protein moiety. As mentioned above, the side chain of Ser31A forms a new hydrogen bond with the OH of Tyr3A, but this interaction is not observed in the B monomer. The main chain nitrogen of Gly32A forms a hydrogen bond interaction with the 2-NH-SO_4^- of the glucosamine moiety of the disaccharide. The main chain nitrogen of a symmetry-related Gly32B also forms a hydrogen bond interaction with this sulfate; this sulfate group of the disaccharide

Table 1. Crystallization of RANTES with Different Heparin Disaccharides

Disaccharide	Crystallization	Concentration	Visible
I-S	Yes	1 mM	Yes
I-A	Yes	1 mM or 10 mM	No
II-S	Yes	1 mM or 10 mM	No
II-A	No	1 mM or 10 mM	No
III-S	Yes	1 mM	Yes

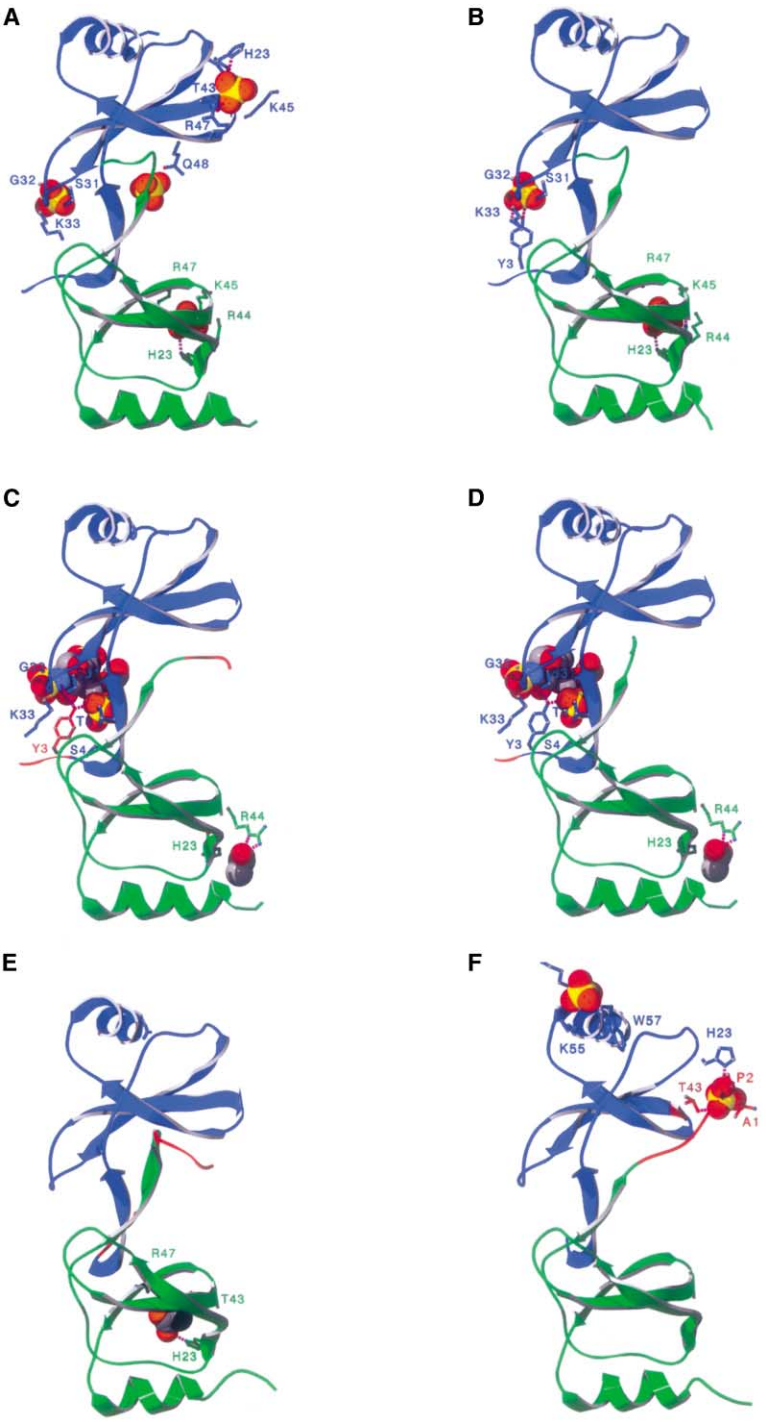

Figure 2. Structure of RANTES Dimers

Ribbon diagrams of dimers with space-filling representation of small molecules in the crystal lattice. Red regions in ribbon diagram correspond to regions of the protein where the position of the C-α differs from that of the AOP-RANTES structure by more than 2 Å. A monomers are colored in blue, and B monomers in green. Side chains of residues interacting with small molecules are shown.

(A) Dimer of AOP-RANTES with sulfate ions.

(B) Dimer of Met-RANTES with sulfate ions.

(C) Dimer of RANTES with heparin disaccharide I-S.

(D) Dimer of RANTES with heparin disaccharide III-S.

(E) Dimer of RANTES-K45E.

(F) Dimer of RANTES-^{44}AANA^{47} with sulfate ions.

is thus sandwiched between two Gly residues of the 30s loop and thereby bridges two RANTES dimers. The K33A side chain swings around substantially due to the movement of Tyr3A and unexpectedly points away from the disaccharide. The Lys33B side chain also points away from the disaccharide, despite being sufficiently close to interact with it. The fact that neither Lys33 side chain interacts with the disaccharides is quite unexpected, since salt bridge interactions would be possible.

None of the residues of the BBXB motif of monomer A interact with the disaccharide, but several interactions are observed with the BBXB motif of the B monomer. The side chain of Arg44B is in an entirely new position, compared to the AOP and Met-RANTES structures, and forms a salt bridge with the 6′-SO_4 group of the disaccharide. This new position can be attributed to the volume occupied by the disaccharide (formerly occupied by the Arg44B side chain) and by the movement of the His23B side chain, which has pushed the Arg44B side chain into its new position. One amino acid side chain

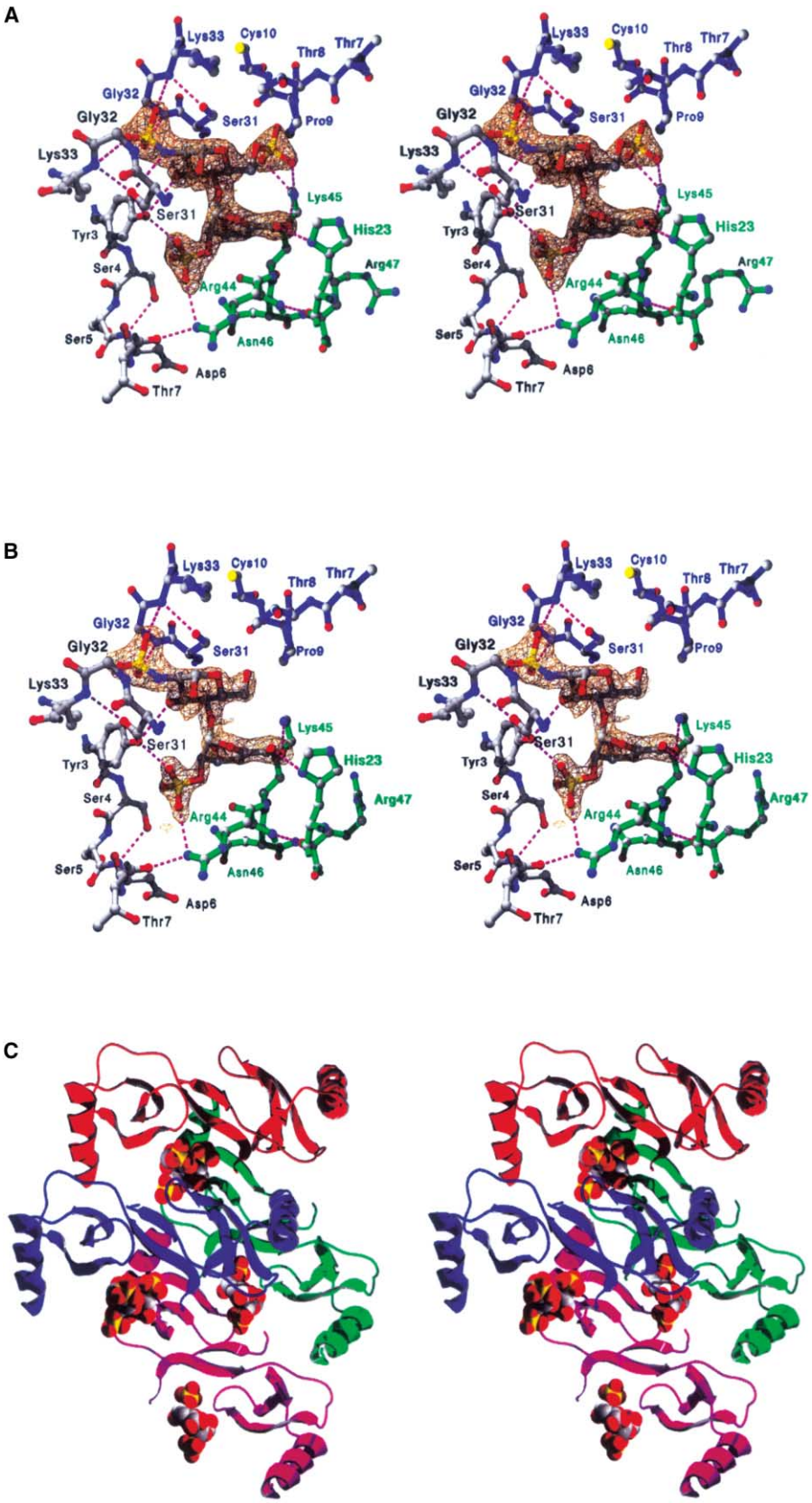

Figure 3. Stereo Diagrams of the Binding Site of Heparin Disaccharides in RANTES Crystals and Crystallographic Lattice

Heparin disaccharide and residues in close proximity are displayed. Carbon atoms colored in gray are from monomer A, those colored in green or blue are from two different symmetry-related B monomers. Putative hydrogen bonds are shown in violet.

(A) Heparin disaccharide I-S with final $2F_o - F_c$ map contoured at 1σ.

(B) Heparin disaccharide III-S with final $2F_o - F_c$ contoured at 1σ.

(C) Crystal lattice of the complex between heparin disaccharide I-S and RANTES. Four dimers of RANTES are displayed.

whose movement may result from the disaccharide binding is His23B. The main chain near residue 23 undergoes some movement, and the His side chain rotates along its Cβ-Cγ bond to allow a salt bridge interaction between the Nδ1 of the imidazol and a carboxylate oxygen of the uronic acid of the disaccharide.

The Lys45B side chain interacts with several atoms of the disaccharide. Two weak hydrogen bonds are formed between the Nϵ and two oxygens of the 6-SO_4 of the glucosamine. These interactions are not present in the RANTES-heparin disaccharide III-S structure due to the lack of the 6-SO_4 group. The Nϵ of Lys45B also forms a salt bridge with the carboxylate group of the uronic acid moiety. While this interaction is conserved in the RANTES-heparin disaccharide III-S, this interaction must be examined with care, due to the non-natural presence of the $\Delta^{4,5}$ double bond.

Structure of RANTES- ^{44}AANA^{47} and Heparin Disaccharides

The crystallization of the RANTES-^{44}AANA^{47} mutant was attempted in the presence of heparin disaccharides with the hope that removal of this primary disaccharide binding domain would permit the binding of a heparin-derived disaccharide to another part of the RANTES molecule, thereby permitting a mapping of the binding region of long chain heparin molecules by sequential mutagenesis. All efforts to produce crystals of this mutant in the presence of heparin disaccharides have proven vain, but the protein did crystallize in the presence of 200 mM $(NH_4)_2SO_4$. Three sulfate ions were observed, two binding to monomer A and one to monomer C (Figure 4F). The first sulfate ion in monomer A binds to the main chain nitrogens of residues Lys56A and Trp57A, but does not interact with the side chains of Lys55A or Lys56A. This sulfate ion also interacts with the side chains of residues of the 50s loop of a symmetry-related RANTES monomer B, with hydrogen bonds to Lys56B and Arg59B. The second sulfate ion binds in the 40s pocket in a position similar to that of the sulfate ion observed in the AOP-RANTES structure, and interacts with the side chains of His23 and Thr43. The sulfate ion in monomer C forms the same interactions with the main chain nitrogens, but also forms a hydrogen bond with the side chain of Lys55C. The interactions with a symmetry-related monomer D 50s pocket are also maintained. These specific interactions with residues of the 50s regions may reveal a putative secondary heparin binding site.

This mutant protein produced crystals with greatly modified packing, apparently due to the role played by the mutated residues in this packing (data not shown), with two dimers of RANTES in the asymmetric unit, related by a noncrystallographic 2-fold symmetry axis roughly parallel to the a axis (data not shown). In the case of wild-type RANTES, the only amino acid of the BBXB motif in the A monomer of the mutant protein that forms important interactions with symmetry-related RANTES molecules is Arg47A, whose side chain forms an important hydrogen bond with the main chain O of Ser65A of a neighboring RANTES molecule. The situation is similar in the B monomer, with only Arg47B forming direct contacts with a neighboring RANTES molecule, through a strong hydrogen bonding between the guanidium group of Arg47B and both the Oϵ1 and the main chain O of Glu66B of the neighboring RANTES molecule (this residue had already been implicated in RANTES oligomerization [Czaplewski et al., 1999]). Thus, only Arg47 in the BBXB motif is implicated in interactions with neighboring molecules, and its absence is probably responsible for the change is crystal packing in the RANTES-^{44}AANA^{47} mutant crystals.

The structure of the RANTES-^{44}AANA^{47} mutant is otherwise essentially unaffected by the mutations. The rms deviation of the position of the main chain atoms of the residues 6–68 of RANTES-^{44}AANA^{47} mutant compared with those of Met-RANTES is only 1.14 Å for the first dimer and 0.99 Å for the second. The region of the mutations in monomer A was poorly defined, and residues Ala44A and Ala45A were not visible in the electron density. The modeling of this region was further complicated by the presence of a sulfate ion in the 40s pocket described above. The 40s loop of the B monomer is well defined and essentially identical to that of wild-type RANTES, as was the case for monomers C and D. The most important movement caused by the mutations occurs in the 20s loop, probably due to the fact that the His23 side chain no longer interacts with residues in the 40s pocket.

Structure of RANTES-K45E

The analysis of the structure of RANTES in the presence of heparin disaccharides suggested a new mutation, which should mimic the results obtained with the RANTES-^{44}AANA^{47}, but which would involve a single amino acid substitution. In this case, Lys45 was mutated to a glutamate residue, producing a charge reversal in the middle of the BBXB motif. The glutamate side chain was expected to prevent the interactions seen between the wild-type RANTES and the heparin disaccharides by sequestering the neighboring Arg44, His23, and Arg47 side chains through salt bridge or hydrogen bonding interactions. This protein was crystallized in the presence of heparin disaccharide I-S, and crystallized in the same space group as the wild-type protein, but the unit cell dimensions were substantially different (Table 2). The overall structure of the protein was unaffected by the mutation, with the exception of the N termini of both monomers, which adopted a configuration similar to that of the B monomer of RANTES in the presence of heparin disaccharide I-S. The 40s loop of RANTES-K45E also underwent some minor movement of the main chain. Unsurprisingly, there was no trace of the heparin disaccharide in the crystal structure. This absence is probably due to the reduced affinity of the mutant protein for heparin oligosaccharides and to the new crystallographic packing, which essentially precludes the presence of the disaccharide molecule near the 40s loop, due to interactions of the latter with neighboring protein molecules.

The mutated Glu45 side chain does form some interesting interactions with the neighboring basic side chains. In the case of the A monomer, the side chain of Glu45A swings toward the interior of the 40s pocket and

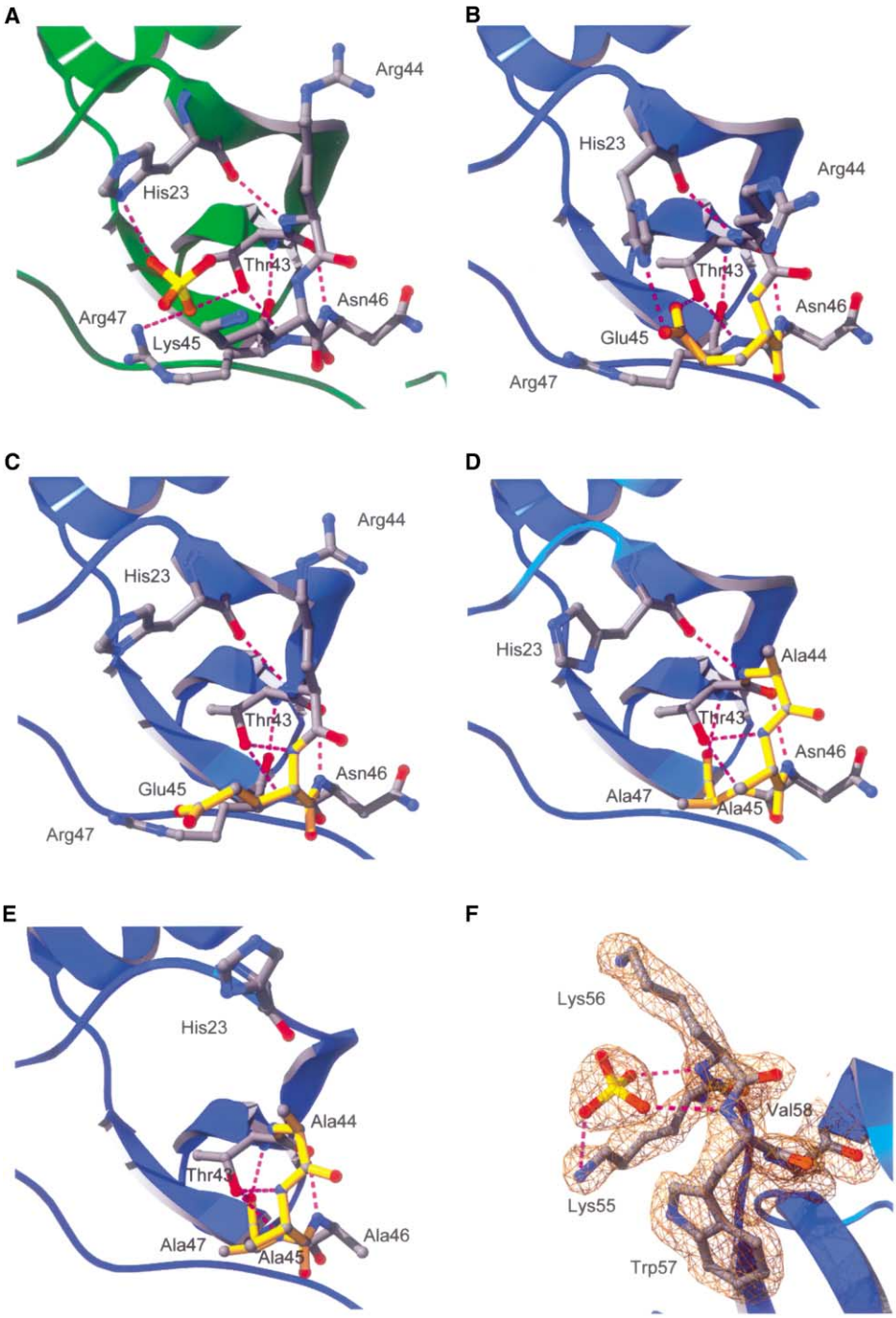

Figure 4. Structure of RANTES Mutants

The carbon atoms of mutated residues are shown in yellow.

(A) Structure of the 40s loop of AOP-RANTES.

(B) Structure of the 40s loop of monomer A of RANTES-K45E.

(C) Structure of the 40s loop of monomer B of RANTES-K45E.

(D) Structure of the 40s loop of monomer C of RANTES-^{44}AANA^{47}.

(E) Structure of 40s loop of monomer D of RANTES-^{44}AANA^{47}.

(F) Structure of RANTES-^{44}AANA^{47} near the sulfate ion binding to the 50s loop. Final $2F_o$-F_c contoured at 1σ.

the carboxylate group forms two hydrogen bond/salt bridge interactions, one with the Oγ of the side chain of Thr43A and one with probably both oxygens of the carboxylate group interacting with the Nϵ of His23A (Figure 4B). This interaction moves the 20s loop substantially closer to the 40s loop than in the wild-type struc-

Table 2. Crystallographic Data on RANTES-Heparin Disaccharide Complexes or Mutants

	HD I-S	HD-IIIS	RANTES-^{44}AANA^{47}	RANTES-K45E
Space group	$P2_12_12_1$	$P2_12_12_1$	$P2_1$	$P2_12_12_1$
a	24.01	24.07	22.82	29.69
b	56.29	56.42	80.48	58.49
c	94.41	95.35	65.44	72.12
β			94.52	
Data Collection				
Resolution range (Å)	20.0–2.0	20.0–2.0	20.0–2.2	20.0–1.7
Total observations	38,679	64,883	32,702	67,032
Independent reflections	9,099	10,362	11,304	13,261
Completeness (%)[1]	98.8 (98.7)	96.0 (90.9)	93.9 (75.0)	91.7 (88.2)
R_{merge} (%)[a,b]	6.5 (19.1)	4.0 (14.9)	8.7 (26.6)	4.6 (8.0)
I/σ[1]	20.3 (6.8)	31.5 (9.5)	11.3 (2.9)	28.9 (18.9)
Refinement				
Resolution range	20.0–2.0	20.0–2.0	20.0–2.2	20.0–1.7
Reflections $> 0.0\sigma$	9,067	8,929	11,269	13,221
R_{factor}[c]	19.8	20.0	22.2	20.6
R_{free} (5% of data)[d]	25.5	25.2	30.6	25.4
Rms deviations				
Bond lengths (Å)	0.005	0.005	0.006	0.004
Bond angles (°)	1.3	1.3	1.3	1.3
Number of atoms				
Protein	1030	1037	2020	1059
Disaccharide	35	31	—	—
Water	159	150	193	310
Other	4	4	15	4
Average B factor				18.2
Protein	21.7	19.9	20.1	14.3
Disaccharide	36.4	35.5	—	—
Water	35.4	32.0	25.8	31.0

[a] Numbers in parentheses refer to the highest resolution shell.
[b] $R_{merge} = \Sigma_{hkl}\Sigma_i|I - \langle I\rangle|/\Sigma_{hkl}\Sigma_i\langle I\rangle$, where I = observed density.
[c] $R_{factor} = \Sigma_{hkl}[|F_{obs}| - \kappa|F_{calc}|]/\Sigma_{hkl}|F_{obs}|$.
[d] R_{free} is the R_{factor} for 5% of the reflections excluded from the refinement.

ture. Contrary to our predictions, the Glu45A does not interact with either Arg44 or Arg47. In the B monomer, the side chain of Glu45A points away from the 40s pocket toward the solvent, and the carboxylate group interacts only with solvent (Figure 4C).

Biological Activity of RANTES Mutants with Impaired Heparin Binding

The analysis of the structure of the complex between RANTES and heparin disaccharides also prompted the preparation of the RANTES mutant Y3A, since, in the crystal structure, this residue interacts strongly with heparin disaccharides. While the structure of this RANTES mutant could not been determined, due to difficulties in obtaining crystals both in the presence and absence of disaccharides, its affinity for a heparin-derived octasaccharide was determined by isothermal fluorescence titration, as was that of the other RANTES mutants, RANTES-^{44}AANA^{47} and RANTES-K45E. While both RANTES-^{44}AANA^{47} and RANTES-K45E display a greatly reduced affinity toward heparin, the RANTES-Y3A mutant maintained a surprising wild-type affinity toward the heparin octasaccharide (Figure 5A). This suggests that the strong interaction observed between the Tyr3A side chain and the heparin disaccharide molecules may either be due to the tight packing in the crystal lattice or may be entirely fortuitous.

Both of these mutants displayed wild-type affinity toward their receptor CCR5 and, contrary to RANTES-^{44}AANA^{47}, which showed a 100-fold drop in potency while achieving full efficacy, displayed wild-type activity in an in vitro chemotaxis assay (data not shown). The capacity of these mutant RANTES molecules to recruit leukocytes in a peritoneal recruitment assay was then measured in order to determine whether the mutants had conserved their biological activity. As shown in Figures 5B and 6C, both the RANTES-K45E and RANTES-Y3A have lost their capacity to recruit cells, as is the case for the RANTES-^{44}AANA^{47} mutant (Proudfoot et al., 2003), thereby confirming the biological importance of the role of Tyr3. Moreover, as we have previously observed for RANTES-^{44}AANA^{47}, these mutants were able to inhibit the ability of RANTES to recruit cells in vivo (Johnson et al., 2004).

Affinity of Heparin and Heparin-Derived Saccharides to RANTES

A study of the relative affinity of RANTES toward heparin-derived disaccharides and heparin molecules was also undertaken by competition equilibrium experiments on immobilized heparin beads using fractionated heparin oligosaccharides ranging in size from disaccharides to 18mers and a commercially available LMW heparin preparation. These studies were also performed against RANTES receptors, CCR1 and CCR5 to determine whether oligosaccharides could compete with the receptors for RANTES binding. Heparin-derived disaccharides were very inefficient in competing for RANTES, requiring milli-

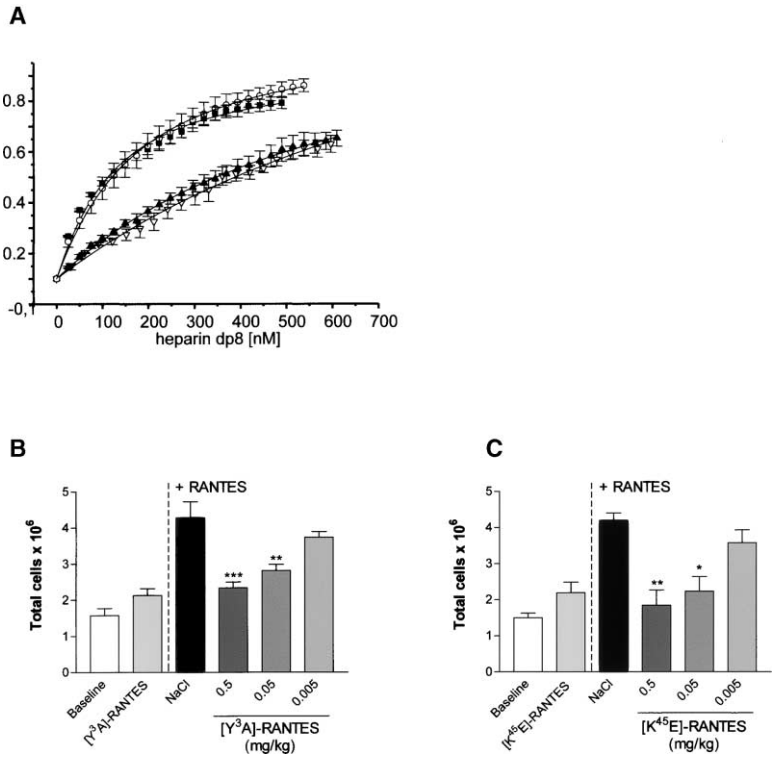

Figure 5. Biochemical Characterization and In Vivo Behavior of RANTES Mutants

(A) Relative affinity of mutant and wild-type RANTES for heparin octasaccharide. Black squares, wild-type RANTES; inverted white triangles, RANTES-^{44}AANA^{47}; black triangles, RANTES-K45E; and white triangles, RANTES-Y3A for a heparin octasaccharide as measured by isothermal fluorescence titrations.

(B) Inhibition by RANTES-Y3A of peritoneal cellular recruitment induced by RANTES. Ten micrograms of RANTES-Y3A is unable to induce peritoneal recruitment (light gray bar). The peritoneal cell recruitment induced by 10 μg of RANTES can be inhibited by RANTES-Y3A in a dose-dependant manner (gray bars).

(C) Inhibition by RANTES-K45E of peritoneal cellular recruitment induced by RANTES. In a similar manner, RANTES-K45E (light gray bars) is unable to induce peritoneal cell recruitment. The peritoneal cell recruitment induced by RANTES (black bar) is also inhibited in a dose-dependent manner by RANTES-K45E (gray bars).

molar concentrations, with the exception of CCR1 where it had an IC_{50} value of 366 μM (Table 3). The higher affinity of the disaccharides for CCR1 could be explained by the fact that the residues in the heparin binding BBXB motif are also involved in CCR1 binding. However, the affinity increases considerably as the heparin chain length increases, since a tetrasaccharide had an IC_{50} of 210, 53, and 304 μM for CCR1, CCR5 and heparin, respectively. The affinities increase with increasing chain length (Table 3), where the 18-mer, displays an IC_{50} value of 1.45 μM toward CCR1, 0.6 μM for CCR5, and 2.4 μM for heparin, similar to results recently reported (Vives et al., 2002). These results suggest that only heparin molecules long enough to occupy more than one pocket in the 40s loop can compete RANTES off the heparin beads. Another hypothesis is that RANTES, when bound to heparin beads, forms a higher order oligomer state, with interactions not only between RANTES and heparin, but also between neighboring RANTES molecules, and the heparin-derived disaccharides are incapable of disrupting this oligomerization

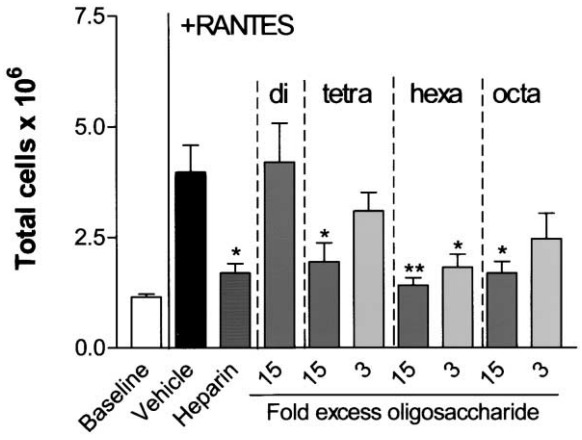

Figure 6. Inhibition of Peritoneal Cellular Recruitment Induced by RANTES by Heparin-Derived Oligosaccharides

The peritoneal cell recruitment induced by 10 μg of RANTES (black bar) can be inhibited by pretreatment, 30 min prior to RANTES injection, by injection of 20 μg of heparin (stippled bar). Pretreatment with a heparin-derived disaccharide at a 15-fold molar excess, compared to the injected RANTES, has no effect on RANTES-mediated cell recruitment. The inhibitory effect of pretreatment with heparin-derived tetra-, hexa- and octasaccharides depends on the molar excess of oligosaccharides.

Table 3. The IC_{50} Values Obtained or Heparin and Heparin-Derived Oligosaccharides by Competition Equilibrium Binding Assays

Number of Saccharides	CCR1	CCR5	Heparin
2	366.00	>1000	>1000
4	210.00	53.00	304.00
6	91.00	44.60	196.00
8	43.00	5.83	18.40
10	5.00	3.54	25.50
12	4.00	1.67	9.20
14	1.80	0.95	4.60
16	1.03	0.74	6.00
18	1.45	0.62	2.40
Heparin[a]	0.06	0.18	2.37

IC_{50} values given in μM.

[a] An average mass of 17.5 kDa was used to calculate the IC_{50} value for the commercially available heparin preparation, which contains heparin with mass between 5 and 30 kDa.

state, contrary to longer heparin molecules. In fact, it is likely that both these phenomena play a role (see below).

The affinity of the fractionated heparin to inhibit RANTES activity was analyzed using the peritoneal cellular recruitment assay in vivo. The purified heparin preparation is able to completely abrogate RANTES induced recruitment at a dose of 20 μg (Figure 6), and the effect is dose dependent (Johnson et al., 2004). A 15-fold excess of heparin tetrasaccharide, hexasaccharide, and octasaccharide were also able to fully inhibit RANTES activity in vivo, while the disaccharide was inactive (Figure 6). The inhibition is dose dependent, since a 3-fold excess of tetrasaccharides did not result in statistically significant inhibition (contrary to longer oligosaccharides), whereas a 15-fold excess did. Thus the results obtained in the in vitro assays were confirmed in vivo, demonstrating that the minimal repeating disaccharide unit is insufficient to inhibit RANTES activity, but molecules such as tetra-, hexa- or octasaccharides are efficient inhibitors.

Discussion

All chemokines studied to date bind heparin in vitro. While this binding is probably due to charge interactions between the generally positively charged chemokines toward the very negatively charged heparin molecules, or other members of the GAG family, the specificity of this interaction is demonstrated by the fact that the two acidic chemokines MIP-1α and MIP-1β do bind heparin, albeit rather weakly (Koopmann and Krangel, 1997; Koopmann et al., 1999). It is believed that binding of chemokines to GAGs is necessary for the development of a chemokine gradient, in order to elicit the recruitment of leukocytes from the circulation, and we have recently formally demonstrated the importance of this interaction for the biological activity of three chemokines in vivo (Proudfoot et al., 2003).

The rapid precipitation of the RANTES protein observed after the addition of many disaccharides suggests that these disaccharides promote rapid oligomerization, similar to what had previously been reported for longer chain heparins (Stura et al., 2002; Koopmann and Krangel, 1997; Wagner et al., 1998). The lack of success in obtaining crystals with both purified heparin-derived tetrasaccharides and hexasaccharides in our hands can probably be attributed to the same reason. We are currently performing crystallization trials on a panel of chemokine mutants that have lost their propensity to oligomerize.

The fact that certain disaccharides were either not visible in the crystal structure or did not permit crystallization reveals some of the features that RANTES requires of the disaccharides, and by extension, to larger heparin molecules. For example, sulfation at the 6-OH of glucosamine is not absolutely required, since the heparin disaccharide III-S, which lacks this sulfate, was not only capable of crystallizing, but was also visible in the crystal lattice. On the other hand, the NH-SO_4^- sulfate group appears to be much more important, since the N-acetylated disaccharides either did not crystallize (HD II-A) or were not visible in the crystal lattice (HD I-A). This is consistent with the estimated binding constants measured by protein NMR using diffusion filters (results not shown) at low pH and using native as well as the two nonaggregating RANTES mutants, which clearly indicated that an N-acetylated heparin disaccharide had a poorer K_d that the N-sulfated equivalent. It is thus also likely that formation of a crystallographic lattice requires the presence of this sulfate group.

Surprisingly, the position of the two sulfate ions in the BBXB pocket of the AOP-RANTES and Met-RANTES does not correspond to the position of any of the sulfates in the disaccharide structures. These sulfate ions thus did not correctly predict the positions of the sulfate groups of the disaccharides. However, the position of the NH-SO_4^- of the glucosamine in the RANTES-disaccharide structures corresponds to the sulfate ion binding to the Ser31A side chain identified in both previously described crystallographic structures. However, the interaction of this NH-SO_4^- with the Oβ of Ser31 appears much weaker, since the new main interaction of the Ser31A side chain is with the OH of Tyr3A.

While crystals of RANTES-^{44}AANA^{47} in the presence of heparin disaccharides could not be obtained, the structure of the protein revealed the presence of three sulfate ions. One of these sulfate ions binds in the 40s pocket of monomer A in a manner similar to that observed in the AOP-RANTES and Met-RANTES, albeit with some important differences probably due to the presence of the three mutated residues. The two new sulfate ions not previously observed in a RANTES crystal both bind to the main chain nitrogens of Arg56A and Arg57A, in monomers A and C in what had already been suspected as being a secondary heparin binding site (Burns et al., 1998). Initial results had indicated that the RANTES mutant RANTES-^{55}AAWVA^{59} displays normal heparin binding in vitro (Proudfoot et al., 2001). These results do not necessarily preclude the role of this region as a secondary weak heparin binding site, since isothermal titration studies have identified a small decrease in the K_d of this RANTES mutant toward heparin (A.K., unpublished data).

Preliminary results on the crystallization of RANTES suggest that conditions that favor oligomerization of RANTES also favor its crystallization. For example, the mutants E66S/A and E26A, which form dimers and tetramers respectively, but which cannot form higher order oligomers (Nichols et al., 2000), do not crystallize. The heavy precipitate observed upon addition of various heparin-derived oligosaccharides to RANTES might be the result of extensive oligomerization. The molecular mass of a RANTES-heparin disaccharide complex exceeds 600 kDa (in which RANTES has a molecular mass of 8 kDa, and the disaccharide a mass of approximately 600 Da), as determined by size exclusion chromatography (results not shown) in conditions very similar to those used for the crystallization of the complex. Extrapolation of this line of reasoning leads to the possibility that the crystal lattice reflects this natural oligomer state of RANTES.

In the crystallographic lattice, 5860A^2 of the RANTES dimer are buried, of the 7740A^2 of total surface area, which corresponds to 76%. Of the 84 amino acids of symmetry-related RANTES molecules in contact with

the RANTES dimer, only three form salt bridges involving their side chains. Two of these salt bridges involve the side chains of Arg47B and Glu66B, and Asp6A and Lys25B, respectively, and are maintained in the heparin disaccharide crystal structure. In the case of the RANTES-disaccharide structures, the important movement of the N terminus of the B monomer disrupts the interaction of Glu66A with the Ser5 side chain observed in the Met-RANTES and AOP-RANTES structures. The interaction of the Glu66B with the Arg47A of a neighboring RANTES dimer is maintained. We initially believed that the Glu66 side chain might therefore play a similar role in both RANTES oligomerization and RANTES crystallization. However, the new crystal lattice, revealed in the structure of the RANTES-^{44}AANA^{47}, suggests that it is Arg47 that is essential for RANTES oligomerization. In the structure of this mutant, the Glu66A and Glu66C side chain forms a new hydrogen bond with a neighboring molecule, but through the Nϵ2 of His23A. This interaction was not present in the wild-type structures, since this His side chain was interacting either with sulfate ions, or heparin disaccharides. Glu66B does not form any interaction with neighboring molecules, and Glu66D forms a new hydrogen bond with the Nϵ of a symmetry-related Lys55. It is likely that the interaction between Glu66 and neighboring molecules is not specific, and that a negatively charged side chain will always find a positively charged partner in such a positively charged molecule such as RANTES. The case for the role of Arg47 in oligomerization is stronger than that of Glu66, since in all RANTES structures obtained so far, this Arg47 always interacts with neighboring RANTES molecules.

The role of heparin binding and oligomerization of RANTES has also been studied by Biacore, by observing the effect of heparin oligosaccharides on a mutant RANTES, lacking residues 1–8, and therefore incapable of dimerizing (Vives et al., 2002). In this study, oligomerization of RANTES could only be caused by the presence of heparin. The binding of RANTES to heparin was observed to implicate two phenomena; oligomerization along the GAG chain and positive cooperativity (i.e., interaction between RANTES molecules). It is probable that several RANTES molecules bind to one heparin chain by interacting not only with the oligosaccharides, but also among themselves. These results are consistent with the results presented here.

It is likely that the binding between heparin and RANTES covers a much larger surface than that observed by the disaccharide structure. This might explain why disaccharides are incapable of efficiently competing for RANTES binding to either its receptors or to immobilized heparin, or inhibit its activity in vivo, despite affinity constants in the micromolar range, while heparin, or fragments as small as tetrasaccharides, are able to prevent cellular recruitment induced by RANTES into the peritoneal cavity. The identification of an important interaction between the disaccharide and the residue Tyr3 at the N terminus, confirmed by mutagenesis as being important for biological activity in vivo, although the heparin binding was unaltered, would suggest an important level of cooperativity between GAG binding and the formation of higher-order complexes. The role of the N terminus region in heparin-induced oligomerization remains to be demonstrated experimentally.

The crystallographic structure of RANTES with heparin disaccharides has provided, to our knowledge, the first structural information concerning this essential interaction and suggests several ways in which this interaction may play a role in RANTES activity. Moreover, examination of the structure allowed the prediction of two mutants, which proved to have the same inhibitory properties of the triple mutant in which the basic residues in the BBXB motif were replaced with neutral Ala residues. In the first case, a single charge reversal mutation of Lys45 was found to be sufficient to result in these inhibitory properties, whereas the second and unexpected mutation at Tyr3 did not impair heparin binding. Whether this residue is involved in heparin induced oligomerization remains to be elucidated. The reason why a heparin-derived tetrasaccharide is capable of fully abrogating the chemotactic response, while a disaccharide is not, is currently being studied. A precise understanding of the molecular basis of these interactions may permit the design of molecules that disrupt the interaction, as demonstrated by the efficacy of a tetrasaccharide in vivo, which could be of use in modulating various inflammatory diseases.

Experimental Procedures

Mutagenesis and Protein Purification

The RANTES mutants RANTES-E26A, Met-RANTES-E66S, RANTES-^{44}AANA^{47}, RANTES-Y3A, and RANTES-K45E, were created by PCR site-directed mutagenesis using a technique based on two mutant primers and two terminal primers. Wild-type and mutant proteins were purified as described (Proudfoot and Borlat, 2002). Heparin and heparin-derived disaccharides were purchased either from Sigma or from Dextra Laboratories. Heparin oligosaccharides were also obtained from Iduron, Manchester UK.

Crystallography

RANTES at 10 mg/ml in 50 mM acetate buffer (pH 3.5) containing the heparin-derived disaccharides (Table 1) at concentrations varying between 0.5 and 10 mM was crystallized at room temperature by hanging drop vapor diffusion. Five microliters of RANTES were mixed with 5 μl of 15% (w/v) PEG 400, 100 mM acetate buffer (pH 4.5), and 10% (w/v) glycerol. Crystals grew over a period of days as thick needles to dimensions of 0.2 $\times$ 0.05 $\times$ 0.05 mm. Prior to freezing directly in the cryostream, crystals were transferred to a cryosolvent solution containing 25% (w/v) PEG 400, 100 mM acetate buffer (pH 4.5), and 10% glycerol and the disaccharide. Crystallographic data was collected at 100 K on an Enraf-Nonius FR591 rotating anode generator equipped with Osmic MaxFlux mirrors and a MAR345 image plate detector. All crystals of wild-type RANTES belong to orthorhombic space group $P2_12_12_1$ with unit cell dimensions a = 24 Å, b = 56 Å, c = 94 Å. Crystals of the mutant RANTES-^{44}AANA^{47} were obtained in the same conditions as the wild-type protein, i.e., 25% PEG 400, 100 mM acetate buffer (pH 4.5), 200 mM $(NH_4)_2SO_4$, and 10% (v/v) glycerol, but belong to space group $P2_1$ with unit cell dimensions a = 22.8 Å, b = 80.5 Å, c = 65.4 Å, with β = 94.5°. RANTES-K45E crystallized in 20% PEG 400 and 100 mM acetate buffer (pH 4.5), but in the absence of $(NH_4)_2SO_4$, and the crystals belonged to space group $P2_12_12_1$, as the wild-type protein crystals, but with different unit cell dimensions: a = 29.7 Å, b = 58.5 Å, c = 72.1 Å. The wild-type protein crystals contain a dimer in the asymmetric unit, as did the RANTES-K45E crystals, whereas the RANTES-^{44}AANA^{47} protein crystals contained two dimers in the asymmetric unit. Data was processed using DENZO and SCALEPACK (Otwinowski and Minor, 1997). Rigid body, simulating annealing, positional and B factor refinement were performed with CNS

(Brunger et al., 1998) and model building with O (Jones et al., 1991). Bulk solvent and anisotropic B factor corrections were applied.

Competition Equilibrium Binding Assays

The affinity of RANTES and its mutants for heparin and heparin-derived oligosaccharides was assessed by the ability of the saccharides to displace iodinated RANTES from immobilized heparin beads according to (Kuschert et al., 1999). The affinity for CCR1 and CCR5 was measured by their ability to displace iodinated RANTES from CHO membranes expressing recombinant receptor using a scintillation proximity assay (Alouani, 2000).

Isothermal Fluorescence Titrations

Steady state fluorescence measurements were performed on a Perkin Elmer (Baconsfield, UK) LS50B fluorimeter according to Falsone et al. (2002) and Goger et al. (2002).

Peritoneal Cell Recruitment

Peritoneal cell recruitment was performed essentially as described in Johnson et al. (2004).

Statistical Tests

Statistically significant inhibition was tested by one-way ANOVA, with a bonferroni post test to compare each treatment with baseline (NaCl). Levels of significance were assigned as follows: $p > 0.05$, ns; *$p < 0.05$; **$p < 0.01$; ***$p < 0.001$.

Received: May 27, 2004
Revised: August 10, 2004
Accepted: August 15, 2004
Published: November 9, 2004

References

Alouani, S. (2000). Scintillation proximity binding assay. Methods Mol. Biol. *138*, 135–141.

Baggiolini, M., Dewald, B., and Moser, B. (1997). Human chemokines: an update. Annu. Rev. Immunol. *15*, 675–705.

Baltus, T., Weber, K.S., Johnson, Z., Proudfoot, A.E., and Weber, C. (2003). Oligomerization of RANTES is required for CCR1-mediated arrest but not CCR5-mediated transmigration of leukocytes on inflamed endothelium. Blood *102*, 1985–1988.

Brunger, A.T., Adams, P.D., Clore, G.M., DeLano, W.L., Gros, P., Grosse-Kunstleve, R.W., Jiang, J.S., Kuszewski, J., Nilges, M., Pannu, N.S., et al. (1998). Crystallography & NMR system: A new software suite for macromolecular structure determination. Acta Crystallogr. D Biol. Crystallogr. *54*, 905–921.

Burns, J.M., Gallo, R.C., DeVico, A.L., and Lewis, G.K. (1998). A new monoclonal antibody, mAb 4A12, identifies a role for the glycosaminoglycan (GAG) binding domain of RANTES in the antiviral effect against HIV-1 and intracellular Ca2+ signaling. J. Exp. Med. *188*, 1917–1927.

Chakravarty, L., Rogers, L., Quach, T., Breckenridge, S., and Kolattukudy, P.E. (1998). Lysine 58 and histidine 66 at the C-terminal alpha-helix of monocyte chemoattractant protein-1 are essential for glycosaminoglycan binding. J. Biol. Chem. *273*, 29641–29647.

Chung, C.W., Cooke, R.M., Proudfoot, A.E., and Wells, T.N. (1995). The three-dimensional solution structure of RANTES. Biochemistry *34*, 9307–9314.

Czaplewski, L.G., McKeating, J., Craven, C.J., Higgins, L.D., Appay, V., Brown, A., Dudgeon, T., Howard, L.A., Meyers, T., Owen, J., et al. (1999). Identification of amino acid residues critical for aggregation of human CC chemokines macrophage inflammatory protein (MIP)-1alpha, MIP-1beta, and RANTES. Characterization of active disaggregated chemokine variants. J. Biol. Chem. *274*, 16077–16084.

Falsone, S.F., Weichel, M., Crameri, R., Breitenbach, M., and Kungl, A.J. (2002). Unfolding and double-stranded DNA binding of the cold shock protein homologue Cla h 8 from Cladosporium herbarum. J. Biol. Chem. *277*, 16512–16516.

Fernandez-Botran, R., Gorantla, V., Sun, X., Ren, X., Perez-Abadia, G., Crespo, F.A., Oliver, R., Orhun, H.I., Quan, E.E., Maldonado, C., et al. (2002). Targeting of glycosaminoglycan-cytokine interactions as a novel therapeutic approach in allotransplantation. Transplantation *74*, 623–629.

Folkard, S.G., Westwick, J., and Millar, A.B. (1997). Production of interleukin-8, RANTES and MCP-1 in intrinsic and extrinsic asthmatics. Eur. Respir. J. *10*, 2097–2104.

Goger, B., Halden, Y., Rek, A., Mosl, R., Pye, D., Gallagher, J., and Kungl, A.J. (2002). Different affinities of glycosaminoglycan oligosaccharides for monomeric and dimeric interleukin-8: a model for chemokine regulation at inflammatory sites. Biochemistry *41*, 1640–1646.

Hoogewerf, A.J., Kuschert, G.S., Proudfoot, A.E., Borlat, F., Clark-Lewis, I., Power, C.A., and Wells, T.N. (1997). Glycosaminoglycans mediate cell surface oligomerization of chemokines. Biochemistry *36*, 13570–13578.

Hoover, D., Shaw, J.P., Gryczynski, Z., Proudfoot, A.E., and Wells, T.N. (2000). The crystal structure of Met-RANTES: Comparison with native RANTES and AOP-RANTES. Protein Pept. Lett. *7*, 200.

Johnson, Z., Kosco-Vilbois, M.H., Herren, S., Cirillo, R., Muzio, V., Zaratin, P., Carbonatto, M., Mack, M., Smailbegovic, A., Rose, M., et al. (2004). Interference with heparin binding and oligomerization creates a novel anti-inflammatory strategy targeting the chemokine system. J. Immunol. *173*, 5776–5785.

Jones, T.A., Zou, J.Y., Cowan, S.W., and Kjeldgaard (1991). Improved methods for building protein models in electron density maps and the location of errors in these models. Acta Crystallogr. A *47* (pt. 2), 110–119.

Koopmann, W., Ediriwickrema, C., and Krangel, M.S. (1999). Structure and function of the glycosaminoglycan binding site of chemokine macrophage-inflammatory protein-1 beta. J. Immunol. *163*, 2120–2127.

Koopmann, W., and Krangel, M.S. (1997). Identification of a glycosaminoglycan-binding site in chemokine macrophage inflammatory protein-1alpha. J. Biol. Chem. *272*, 10103–10109.

Kuschert, G.S., Coulin, F., Power, C.A., Proudfoot, A.E., Hubbard, R.E., Hoogewerf, A.J., and Wells, T.N. (1999). Glycosaminoglycans interact selectively with chemokines and modulate receptor binding and cellular responses. Biochemistry *38*, 12959–12968.

Laurence, J.S., Blanpain, C., Burgner, J.W., Parmentier, M., and LiWang, P.J. (2000). CC chemokine MIP-1 beta can function as a monomer and depends on Phe13 for receptor binding. Biochemistry *39*, 3401–3409.

Martin, L., Blanpain, C., Garnier, P., Wittamer, V., Parmentier, M., and Vita, C. (2001). Structural and functional analysis of the RANTES-glycosaminoglycans interactions. Biochemistry *40*, 6303–6318.

Nichols, A., Camps, M., Gillieron, C., Chabert, C., Brunet, A., Wilsbacher, J., Cobb, M., Pouyssegur, J., Shaw, J.P., and Arkinstall, S. (2000). Substrate recognition domains within extracellular signal-regulated kinase mediate binding and catalytic activation of mitogen-activated protein kinase phosphatase-3. J. Biol. Chem. *275*, 24613–24621.

Otwinowski, Z., and Minor, W. (1997). Processing of X-ray diffraction data collected in oscillation mode. In Methods in Enzymology, Volume 276: Macromolecular Crystallography, Part A, C.W. Carter, Jr. and R.M. Sweet, eds. (New York: Academic Press), 307–326.

Paavola, C.D., Hemmerich, S., Grunberger, D., Polsky, I., Bloom, A., Freedman, R., Mulkins, M., Bhakta, S., McCarley, D., Wiesent, L., et al. (1998). Monomeric monocyte chemoattractant protein-1 (MCP-1) binds and activates the MCP-1 receptor CCR2B. J. Biol. Chem. *273*, 33157–33165.

Proudfoot, A.E., and Borlat, F. (2002). Chemokine Protocols. (Humana Press, Towota, NJ).

Proudfoot, A.E., Fritchley, S., Borlat, F., Shaw, J.P., Vilbois, F., Zwahlen, C., Trkola, A., Marchant, D., Clapham, P.R., and Wells, T.N. (2001). The BBXB motif of RANTES is the principal site for heparin binding and controls receptor selectivity. J. Biol. Chem. *276*, 10620–10626.

Proudfoot, A.E., Handel, T.M., Johnson, Z., Lau, E.K., LiWang, P.,

Clark-Lewis, I., Borlat, F., Wells, T.N., and Kosco-Vilbois, M.H. (2003). Glycosaminoglycan binding and oligomerization are essential for the in vivo activity of certain chemokines. Proc. Natl. Acad. Sci. USA *100*, 1885–1890.

Rajarathnam, K., Sykes, B.D., Kay, C.M., Dewald, B., Geiser, T., Baggiolini, M., and Clark-Lewis, I. (1994). Neutrophil activation by monomeric interleukin-8. Science *264*, 90–92.

Robinson, E., Keystone, E.C., Schall, T.J., Gillett, N., and Fish, E.N. (1995). Chemokine expression in rheumatoid arthritis (RA): evidence of RANTES and macrophage inflammatory protein (MIP)-1 beta production by synovial T cells. Clin. Exp. Immunol. *101*, 398–407.

Rossi, D., and Zlotnik, A. (2000). The biology of chemokines and their receptors. Annu. Rev. Immunol. *18*, 217–242.

Skelton, N.J., Aspiras, F., Ogez, J., and Schall, T.J. (1995). Proton NMR assignments and solution conformation of RANTES, a chemokine of the C–C type. Biochemistry *34*, 5329–5342.

Spillmann, D., Witt, D., and Lindahl, U. (1998). Defining the interleukin-8-binding domain of heparan sulfate. J. Biol. Chem. *273*, 15487–15493.

Stringer, S.E., and Gallagher, J.T. (1997). Specific binding of the chemokine platelet factor 4 to heparan sulfate. J. Biol. Chem. *272*, 20508–20514.

Stringer, S.E., Forster, M.J., Mulloy, B., Bishop, C.R., Graham, G.J., and Gallagher, J.T. (2002). Characterization of the binding site on heparan sulfate for macrophage inflammatory protein 1alpha. Blood *100*, 1543–1550.

Stura, E.A., Martin, L., Lortat-Jacob, H., Vives, R., and Vita, C. (2002). Heparin-aggregated RANTES can be crystallised. Acta Crystallogr. D Biol. Crystallogr. *58*, 1670–1673.

Sweeney, E.A., Lortat-Jacob, H., Priestley, G.V., Nakamoto, B., and Papayannopoulou, T. (2002). Sulfated polysaccharides increase plasma levels of SDF-1 in monkeys and mice: involvement in mobilization of stem/progenitor cells. Blood *99*, 44–51.

Vives, R.R., Sadir, R., Imberty, A., Rencurosi, A., and Lortat-Jacob, H. (2002). A Kinetics and Modeling Study of RANTES(9–68) Binding to Heparin Reveals a Mechanism of Cooperative Oligomerization. Biochemistry *41*, 14779–14789.

Wagner, L., Yang, O.O., Garcia-Zepeda, E.A., Ge, Y., Kalams, S.A., Walker, B.D., Pasternack, M.S., and Luster, A.D. (1998). Beta-chemokines are released from HIV-1-specific cytolytic T-cell granules complexed to proteoglycans. Nature *391*, 908–911.

Wilken, J., Hoover, D., Thompson, D.A., Barlow, P.N., McSparron, H., Picard, L., Wlodawer, A., Lubkowski, J., and Kent, S.B. (1999). Total chemical synthesis and high-resolution crystal structure of the potent anti-HIV protein AOP-RANTES. Chem. Biol. *6*, 43–51.

Accession Numbers

Atomic coordinates for the structure of the complex RANTES-heparin disaccharide I-S, RANTES-heparin disaccharide III-S, RANTES-K45E, and RANTES-^{44}AANA^{47} have been deposited in the Protein Data Bank with accession codes 1u4l, 1u4m, 1u4p, and 1u4r, respectively.